Electronic supplementary information

Self-assembled growth of Pd-Ni sub-microcages as a highly active and durable electrocatalyst

Ming Zhao,[a,*] Zinan Kang,[a] Qiang Chen,[b] Xinxin Yu,[c] Yanfang Wu,[a] Xing Fan,[a] Xinlong Yan,[a] Yue Lin,[d,*] Tian Xia[a], Weiwei Cai[c]

[a]School of Chemical Engineering, China University of Mining and Technology, No.1, Daxue Road, Xuzhou 221116, China

[b]School of Chemical Engineering and Technology, Xi'an Jiaotong University, Xi'an, Shaanxi 710049, China

[c]Sustainable Energy Laboratory, Faculty of Materials Science and Chemistry, China University of Geosciences (Wuhan), Wuhan 430074, China

[d]Hefei National Laboratory for Physical Sciences at the Microscale, University of Science and Technology of China, Hefei, Anhui 230026, China

Email: ming815zhao@163.com; linyue@ustc.edu.cn

1. Chemicals Palladium (II) acetylacetonate [$Pd(acac)_2$, 99%], nickel(II) acetylacetonate [$Ni(acac)_2$, 95%], triphenylphosphine, ReagentPlus® (TPP, 99%), tetrabutylammonium bromide, ReagentPlus (TBAB, 99%), trioctylphosphine oxide (TOPO, technical grade 90%), borane *tert*-butylamine complex (BTB, 97%), oleic acid (OA, technical grade 90%), oleylamine (OLA, technical grade 70%), and nafion perfluorinated ion-exchange resin (5 wt % solution in a lower aliphatic alcohol/H_2O mixture that contains 15-20% water) were purchased from Sigma-Aldrich Co.; activated carbon (Vulcan XC-72) was purchased from Moubic INC.; activated carbon supported Pt-Ru NPs (20 wt% Pt and 10 wt% Ru, Johnson Matthey Corp.) was purchsed from Alfa-Aesar Co. The carbon mentioned in this paper is activated carbon (Vulcan XC-72) in all cases. All the reagents were used without further purification.

2. Apparatus Transmission electron microscopy (TEM) and high-resolution TEM (HRTEM) were performed on a Tecnai G2 F20 S-TWIN with accelerating voltage of 200 kV. Scanning electron microscopy (SEM) was performed on a GeminiSEM 500. Atomic resolution high-angle annular dark-field (HAADF) images were obtained using an aberration-corrected (S)TEM (JEM ARM200F) operating at 200 kV. Energy Dispersive Spectroscopy (EDS) mappings were taken with a super X-EDS system (four silicon drift detectors arranged systematically) on FEI Talos F200X at 200 kV. X-ray diffraction (XRD) was performed on a D8 Advance instrument. X-ray photoelectron spectrometer (XPS) was performed on a ESCALAB 250Xi. The compositions of the materials were determined by laser ablation inductively coupled plasma mass (LA-ICP-MS) using an Agilent NWR

213-7900 instrument. Brunauer-Emmett-Teller (BET) surface area and Barrett-Joyner-Halenda (BJH) measurements for all the materials (including activated carbon as the support) were performed by nitrogen sorption isotherms using a Autosotrb-IQ2-MP-XR.

3. Electrochemical Experiments Cyclic voltammogram (CV) and Electrochemical impedance spectra (EIS) experiments were performed on a CHI660 electrochemical analyzer supplied by CH Instruments Ins. A conventional three-electrode cell was used, including a Hg/Hg_2Cl_2 (saturated KCl) electrode as the reference electrode, a platinum wire as the counter electrode, and a modified glassy carbon electrode (GCE) (with a surface area of 0.07 cm^2, BAS Inc.) as the working electrode. The potential value used in CV and LSV profiles were changed from $E(Hg/Hg_2Cl_2)$ to E(RHE), according to the formula $E(RHE) = E(Hg/Hg_2Cl_2) + 0.2412$ volts + 0.05916 × pH volts. For the electro-catalyst preparation, a mixture of catalyst (around 2 mg), nafion (10 μL), distilled H_2O (95 μL), and ethanol (95 μL) was ultrasonically dispersed for 20 min to form an ink. The modified GCE was coated with the as-obtained catalyst ink (6 μL) and dried naturally at room temperature. The CV measurements for electrochemical surface areas were performed in N_2-saturated 0.5 M KOH (aqueous) at a scan rate of 50 mV/s at 298 K. The CV experiments for methanol oxidation were performed in 0.5 M KOH (aqueous) that contained 1.0 M MeOH at a scan rate of 50 mV s^{-1} at 298 K. To study the MOR on the catalysts, the electrode was first subjected to continuous potential cycling between 0.26 and 1.35 V (versus RHE) at a rate of 50 mV s^{-1} in an aqueous solution of 0.5 M KOH and 1 M MeOH until stabilized voltammograms were obtained. Impedance spectra were measured in a frequency range of 10^{-1} to 10^4 Hz at five points per frequency decade with an amplitude of 50 mV.

4. Fabrication of Pd-Ni MCs-2 mixed with carbon A mixture of palladium acetylacetonate (0.2 mmol), nickel acetylacetonate (0.2 mmol), TPP (0.88 mmol), TBAB (1.5 mmol), and TOPO (3 mmol) was deaerated using nitrogen gas for 20 min. After that, the reaction solution was heated to 220 °C at a constant heating rate of 12 °C min^{-1} and kept at 220 °C for 30 min. Then, the mixture was heated to 280 °C and incubated for 15 min. After cooling to room temperature, the mixture was diluted with ethanol. The resulting Pd-Ni particle aggregates were separated by centrifugation (13000 rpm for 10 min) and wash with ethanol twice and then dispersed in hexane. In a round-bottom flask, a suspension of Vulcan XC-72 in hexane (50 mg in 100 mL) was subjected to ultrasonication for 25 min, into which the Pd-Ni particle aggregates were added. The mixture was subjected to ultrasonication for another 25 min. After evaporation of hexane, the remaining material was calcined at 300 °C under nitrogen gas for 2 h to give the desired supported Pd-Ni MCs-2.

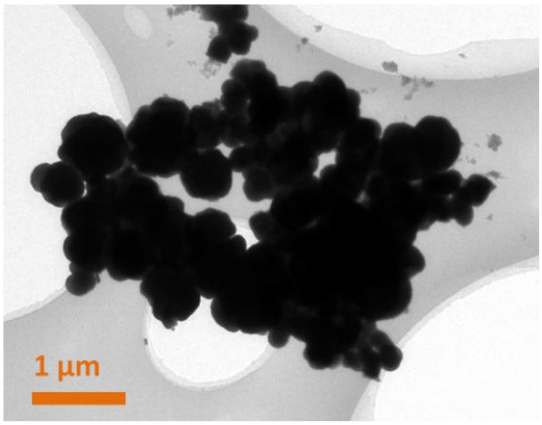

Fig. S1 TEM image of the aggregates of small Pd-Ni NPs.

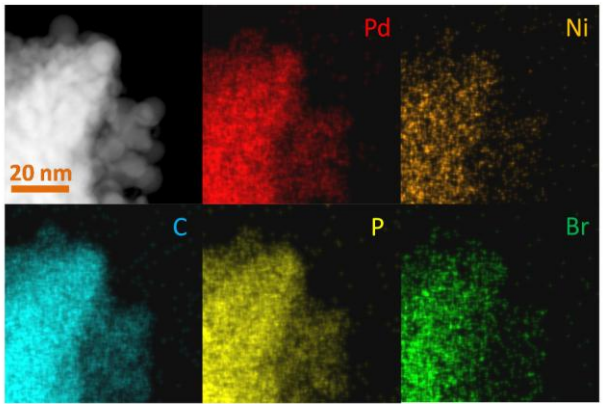

Fig. S2 STEM and EDX-Mapping images of the aggregates of small Pd-Ni NPs.

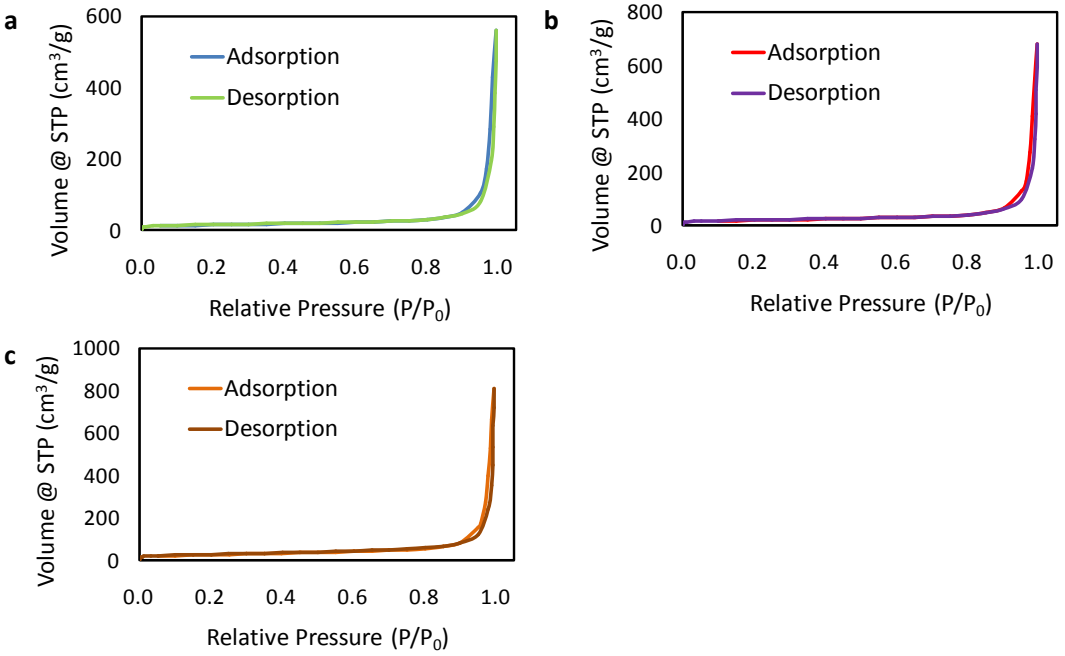

Fig. S3 Nitrogen adsorption and desorption isotherm of the materials fabricated with different amount of TOPO: (2.0 mmol for **a**), (3.0 mmol for **b**), and (4.5 mmol for **c**). Noted that activated carbon was used as the support in all cases.

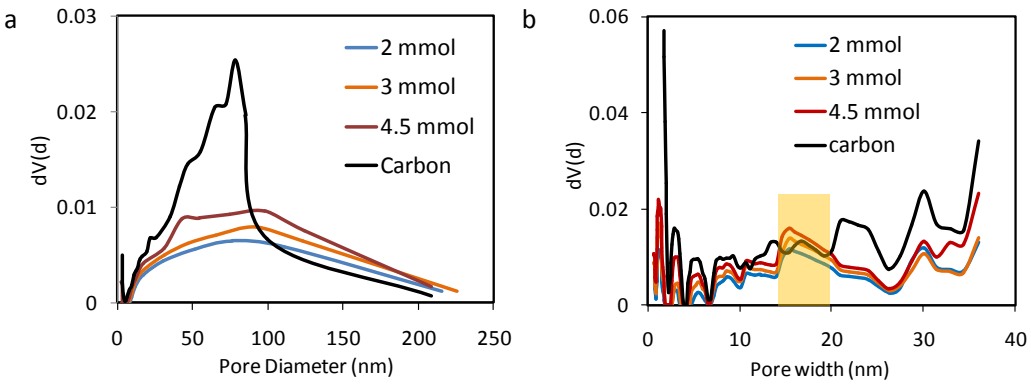

Fig. S4 Pore size distribution analysis of activated carbon and three types of Pd-Ni MCs fabricated with different amount of TOPO based on the Barrett-Joyner-Halenda (BJH, a) and density functional theory (DFT, b) methods.

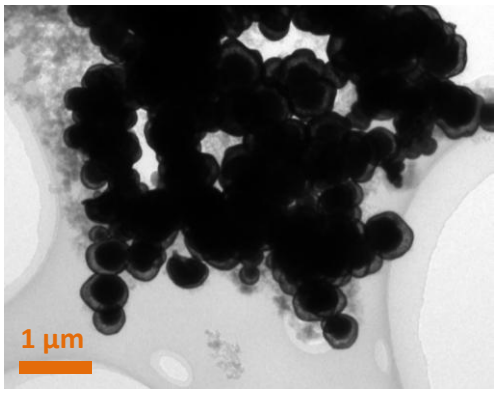

Fig. S5 TEM image of the referenced yolk shell sub-microparticles fabricated with 1.0 mmol TBAB.

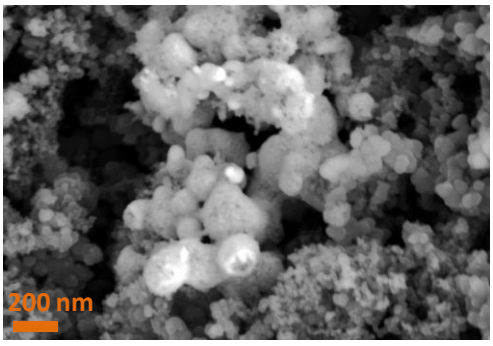

Fig. S6 SEM image of the synthesized materials in the absence of TPP.

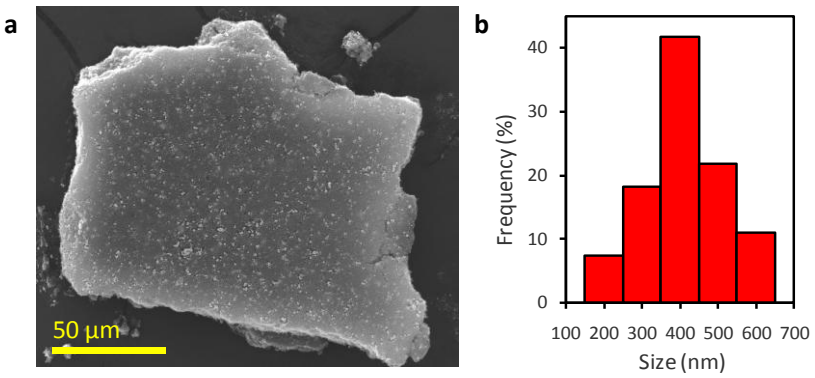

Fig. S7 (a) Low resolution SEM image of Pd-Ni MCs-2 with carbon. (b) Size distribution of Pd-Ni MCs.

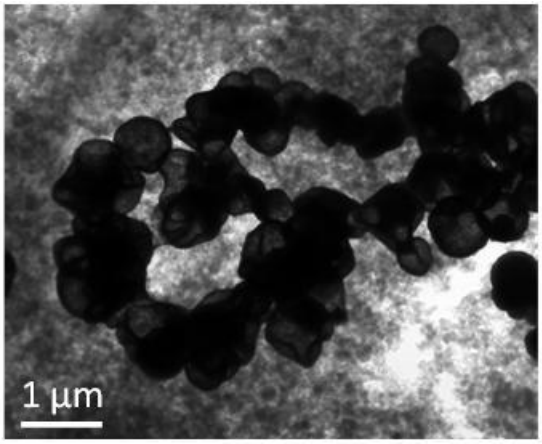

Fig. S8 TEM image of Pd-Ni MCs-2 with carbon.

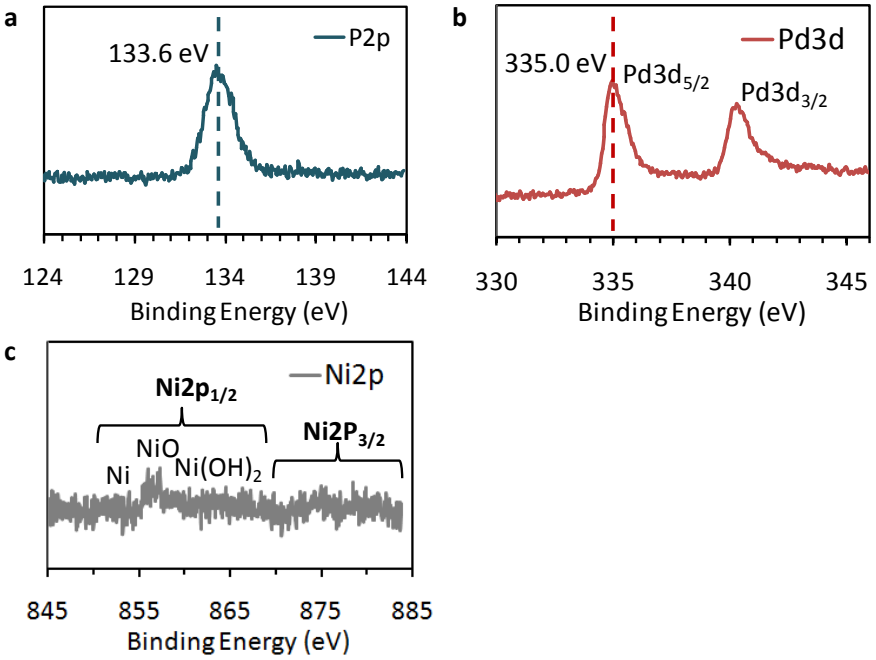

Fig. S9 XPS spectra of Pd-Ni MCs-2 in terms of P2p (a), Pd3d (b) and Ni2p (c).

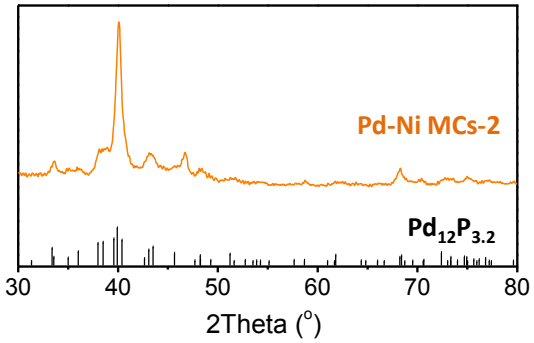

Fig. S10 XRD patterns of the supported Pd-Ni MCs-2 and the $Pd_{12}P_{3.2}$ reference (PDF#42-0922).

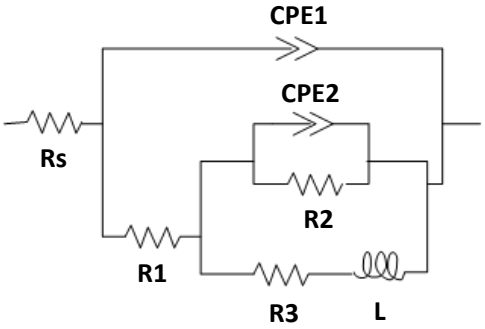

Fig. S11 Equivalent circuits compatible with the experimental impedance data in Fig. 5a and Fig. 6c for methanol electro-oxidation at 0.75 V.

Table S1. Equivalent circuit parameters of electrooxidation of methanol in KOH solution obtained from Fig. 5a and Fig. 6c. All the materials mentioned here were supported on carbon.

	Pd-Ni MCs-1	Pd-Ni MCs-2	Pd-Ni MCs-3	Pd-Ni NPs
R_s	15.41	14.98	14.77	27.52
R_1	9.915	26.04	20.98	27.05
R_3	5.19E+02	388.7	198.8	1920
CPE_2 (Q_2)	0.93205	0.99029	0.94291	0.94126
R_2	357.3	408.8	188.2	1356
CPE_1 (Q_1)	0.9116	0.83164	0.85433	0.83509

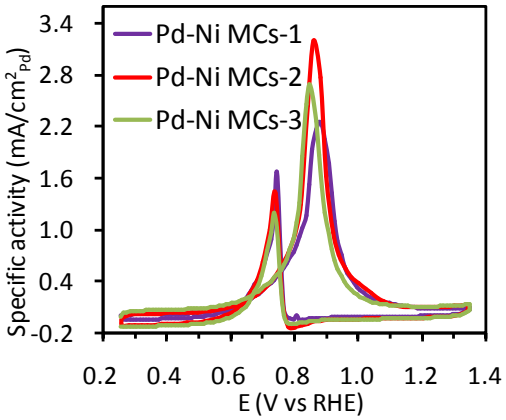

Fig. S12 Comparisons of the specific activities of different MCs in MOR. CV experiment was performed in 1.0 M MeOH and 0.5 M KOH under room temperature at a scan rate of 50 mV/s.

5. Fabrication of carbon supported Pd-Ni NPs

In a three-neck flask with reflux apparatus, a mixture of $Pd(acac)_2$ (0.35 mmol), $Ni(acac)_2$ (0.01 mmol), TBAB (1.0 mmol), and TOPO (3.0 mmol) were dissolved in OLA (6.0 mL) at room temperature, and the mixture was stirred for 30 min under a nitrogen flow. The reaction solution was heated to 220 °C at a constant heating rate of 12 °C min^{-1} and kept at 220 °C for 30 min. Then, it was heated to 270 °C with a heating rate of 15 °C min^{-1}, and kept at that temperature for 15 min. After the reactants were cooled down to room temperature, added 40 mL of ethanol. Centrifugation (10000 rpm) for 8 min gave Pd-Ni NPs coated by OLA as the precipitation, which was washed with ethanol (30 mL) carefully. The resulting material was disperse and kept in toluene.

For the fabrication of Pd-Ni/C: In a round-bottom flask, a suspension of activated carbon in toluene (70 mg in 140 mL) was under ultrasonic for 25 min, to which a solution of as-synthesized Pd-Ni NPs in toluene (30 mg in 120 mL) was added. After that, the mixture went through ultrasonic for another 25 min. After evaporated to remove toluene, the mixture was calcined at 300 ^{o}C under nitrogen gas for 2 h. LA-ICP-MS analysis determined the composition of the NPs as $Pd_{35.5}Ni_1$. The material was characterized by TEM as shown in Fig. S11.

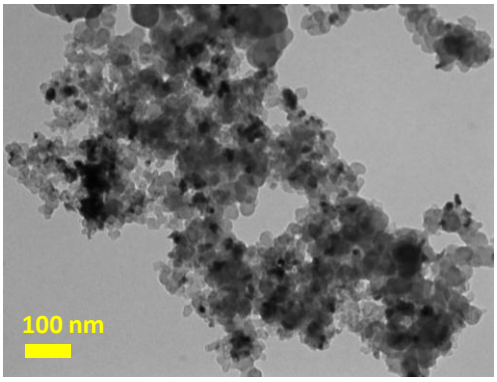

Fig. S13 TEM image of carbon supported Pd-Ni NPs.

6. Fabrication of carbon supported Pd NPs

The Pd NPs were fabricated according to the previous method reported by Hyeon.[S1] For the fabrication of Pd/C: In a round-bottom flask, a suspension of activated carbon in toluene (70 mg in 140 mL) was under ultrasonic for 25 min, to which a solution of as-synthesized Pd NPs in toluene (30 mg in 120 mL) was added. After that, the mixture went through ultrasonic for another 25 min. After evaporated to remove toluene, the mixture was calcined at 300 ^{o}C under nitrogen gas for 2 h. The material was characterized by TEM and HRTEM as shown in Fig. S12.

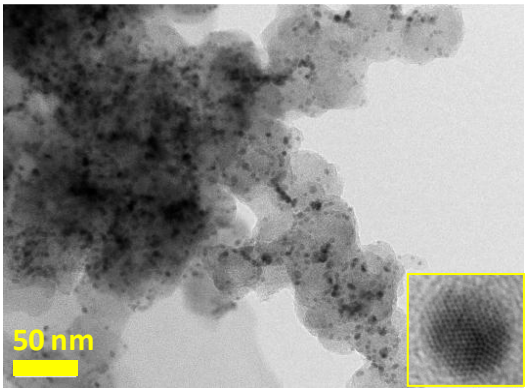

Fig. S14 TEM and HRTEM (inset) images of Pd NPs supported on carbon.

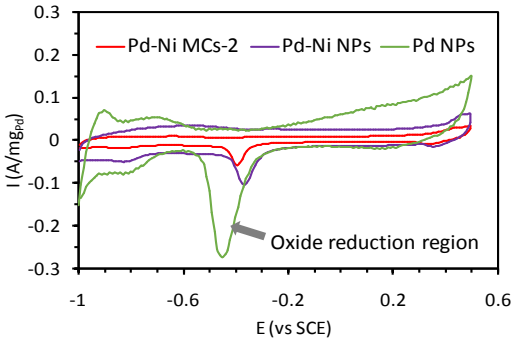

Fig. S15 CV curves of various Pd-based catalysts in deaerated 0.5 M KOH (aq). The electro-chemical surface areas (ECSAs) of catalysts were calculated based on the formula *ECSA* $(m^2/g) = Q\ (mC)/[0.405\ mC{\cdot}cm^2 \times W_{Pd}\ (mg) \times 10]$. *Q* represents the charge by integrating the Pd oxide reduction region after double-layer correction, and W_{Pd} is the mass amount of Pd loaded on the working electrode.

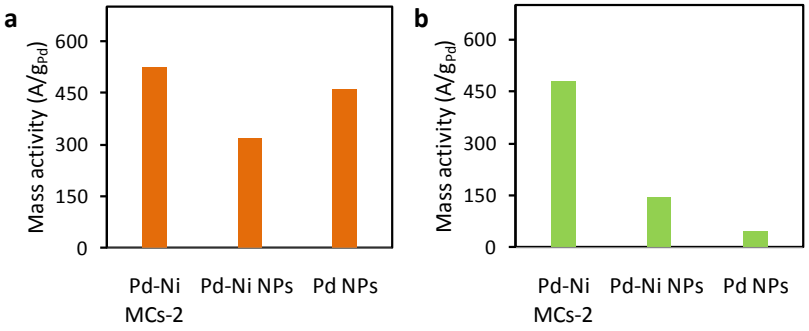

Fig. S16 Comparison of mass activity of different Pd-based catalysts before (a) and after (b) 2000 CVs.

Table S2. The onset potential, over potential, and I_f/I_b ratio summarized from Fig. 6h.

Cycle number	Onset potential (mV)	Over potential (mV)	I_f/I_b ratio
1st	580	860	2.3
2000th	600	860	2.4

Table S3. Comparisons of the activities and stabilities of different electro-catalysts in MOR.

Catalyst	Electrolyte	Specific activity (mA/cm^2)	Mass activity (A/mg)	**Number of cycles**	**Durability (mA/mg)**	Reference
Pd-Ni MCs-2	**0.5 M KOH + 1 M CH_3OH**	**3.2**	**0.53**	**2000**	**480**	**This work**
Pd-Ni-P/C (8 nm)	0.5 M KOH + 1 M CH_3OH	0.6	0.36	**400**	**352**	S2
Pd/RGO	1 M KOH + 1 M CH_3OH	0.6	0.37	**400**	**70**	S3
Pd_1Ru_1 NFs	1 M KOH + 1 M CH_3OH	4.2	1.28	**500**	**480**	S4
Pd-Ni nanospheres	1 M KOH + 1 M CH_3OH	2.0	0.62	**500**	**440**	S5
$Pd_3RuP_{1.5}$	1 M KOH + 1 M CH_3OH	2.3	1.30	**500**	**710**	S6
NiCoPd/CNTs	1 M NaOH + 1 M CH_3OH	1.7	0.86	**500**	**840**	S7
NPG@Pd	0.5 M KOH + 1 M CH_3OH	2.1	-	**1000**	**-**	S8
PdAu-P	0.1 M KOH + 0.5 M CH_3OH	1.1	0.40	**1000**	**310**	S9
PdAu NWs	0.5 M NaOH + 1 M CH_3OH	0.9	0.53	**1000**	**440**	S10
PdAu-1	1 M NaOH + 1 M CH_3OH	4.0	0.21	**1000**	**180**	S11
3D-2D PdRu/NiZn oxyphosphide nanohybrids	1 M KOH + 1 M CH_3OH	4.5	1.74	**1000**	**1250**	S12

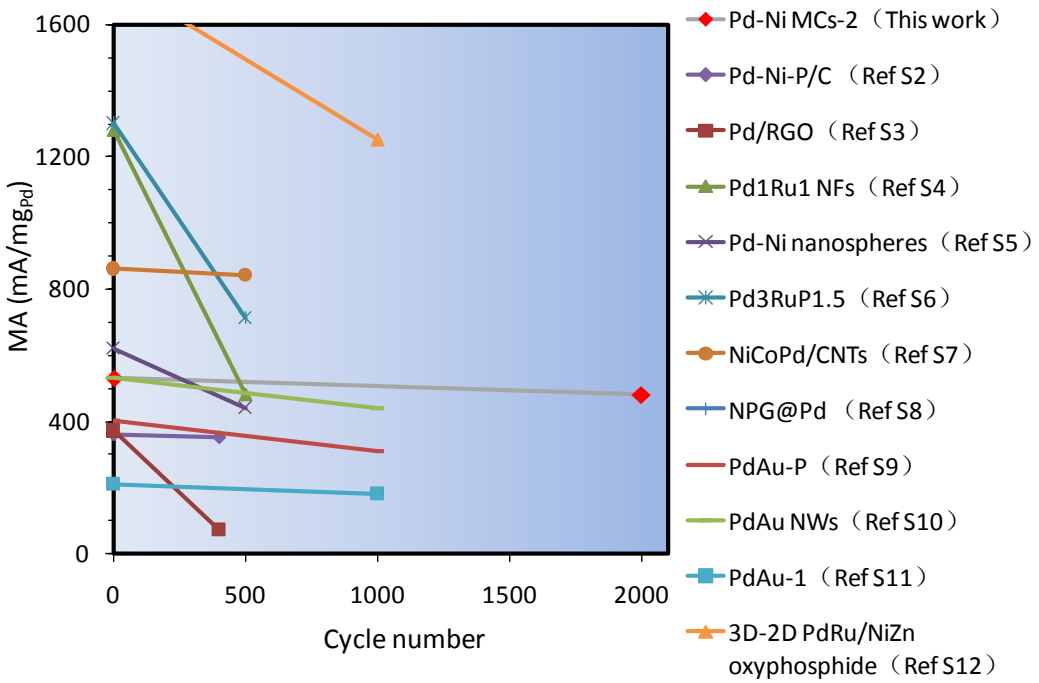

Fig. S17 Comparisons of the changes on mass activity of different Pd-based catalysts before and after various CVs.

Reference

S1. S. W. Kim, J. Park, Y. Jang, Y. Chung, S. Hwang, T. Hyeon and Y. W. Kim, *Nano Lett.*, 2003, **3**, 1289-1291.

S2. M. Zhao, K. Abe, S. Yamaura, Y. Yamamoto and N. Asao, *Chem. Mater.*, 2014, **26**, 1056-1061.

S3. Y. Wang, Y. Zhao, J. Yin, M. C. Liu, Q. Dong and Y. Q. Su, *Int. J. Hydrogen Energy*, 2014, **39**, 1325-1335.

S4. H. Xu, B. Yan, K. Zhang, J. Wang, S. M. Li, C. Q. Wang, Y. Shiraishi, Y. K. Du and P. Yang, *J. Colloid Interface Sci.*, 2017, **505**, 1-8.

S5. Z. L. Gu, H. Xu, D. Bin, B. Yan, S. M. Li, Z. P. Xiong, K. Zhang and Y. K. Du, *Colloid Surface A*, 2017, **529**, 651-658.

S6. H. Xu, B. Yan, K. Zhang, C. Q. Wang, J. T. Zhong, S. M. Li, P. Yang and Y. K. Du, *Int. J. Hydrogen Energy*, 2017, **42**, 11229-11238.

S7. J. W. Zhang, B. Zhang and X. Zhang, *J. Solid State Electrochem.*, 2017, **21**, 447-453.

S8. Y. Xu, P. M. Yiu, G. C. Shan, T. Shibayama, S. Watanabe, M. Ohnuma, W. Huang and C. H. Shek, *Chemnanomat*, 2018, **4**, 88-97.

S9. T. F. Li, Y. Wang, Y. Z. Tang, L. Xu, L. Si, G. T. Fu, D. M. Sun and Y. W. Tang, *Catal. Sci. Technol.*, 2017, **7**, 3355-3360.

S10. Q. L. Wang, R. Fang, L. L. He, J. J. Feng, J. H. Yuan and A. J. Wang, *J. Alloys Compd.*, 2016, **684**, 379-388.

S11. L. M. Luo, R. H. Zhang, J. J. Du, F. Yang, H. M. Liu, Y. Yang and X. W. Zhou, *Int. J. Hydrogen Energy*, 2017, **42**, 16139-16148.

S12. H. Xu, P. P. Song, Y. P. Zhang and Y. K. Du, *Nanoscale*, 2018, **10**, 12605-12611.